ISSN 1075-7015, Geology of Ore Deposits, 2021, Vol. 63, No. 1, pp. 34–53. © Pleiades Publishing, Ltd., 2021.
Russian Text © The Author(s), 2021, published in Geologiya Rudnykh Mestorozhdenii, 2021, Vol. 63, No. 1, pp. 40–61.

Burgali Epithermal Au–Ag Deposit in the Paleozoic Kedon Volcanic Belt (Northeastern Russia)

A. V. Volkov[a], *, N. E. Savva[b], B. I. Ishkov[c], A. A. Sidorov[a], E. E. Kolova[b], and K. Yu. Murashov[a]

[a] *Institute of Geology of Ore Deposits, Petrography, Mineralogy, and Geochemistry, Russian Academy of Sciences, Moscow, 119017 Russia*

[b] *Northeastern Interdisciplinary Scientific Research Institute, Far East Branch, Russian Academy of Sciences, Magadan, 685010 Russia*

[c] *ZAO Omolon Gold Mining Company, Magadan, 685000 Russia*

**e-mail: tma2105@mail.ru*

Received December 19, 2019; revised April 16, 2020; accepted April 18, 2020

Abstract—The Burgali deposit is located in the Paleozoic Kedon volcanic belt (KVB) within the Omolon cratonic terrane. The orebodies of the Burgali deposit are veined and stockwork-type. The studies of the wallrock metasomatites demonstrate that the erosional truncation of the deposit is close to minimal. The ores of the deposit are enriched in the chalcophile elements (Au, Ag, As, Sb, Te, W, Mo, and Bi) and poor in the rare earths. The rare-earth element (REE) spectra are dominated by light lanthanides. The ores are characterized as very low-sulfidation with finely disseminated mineralization, widespread occurrence of chalcedony, and widespread colloform-banded, often combined with brecciated, structures. The late quartz veins contain Lower Carboniferous coaly siltstone fragments, filled with petrified timber remains, which indicate the Carboniferous age of the ore mineralization. The ores contain widespread Au- and Te-bearing pearceite and rare minerals such as argyrodite and the selenous petrovskaite and uytenbogaardtite. The data obtained enable the Burgali deposit to be classified as low-sulfidation epithermal. The outlook for Ag and Au reserve additions is based on the further studies and exploration of the ore-bearing stockwork.

Keywords: northeastern Russia, Omolon terrane, Paleozoic Kedon volcanic belt, Burgali epithermal Au–Ag deposit, geological structure, mineralogy, geochemistry, ores

DOI: 10.1134/S1075701520060082

INTRODUCTION

The Paleozoic epithermal Au–Ag deposits of northeastern Russia are concentrated in the preaccretion Kedon volcanic belt (KVB) within the Omolon cratonic terrane (Fig. 1). The low sulfidation distinguishes the ores of these deposits from their Late Mesozoic equivalents in the Okhotsk–Chukotka volcanic belt (OCVB) (Volkov et al., 2011).

The Burgali deposit is located in the Severo-Evensk district of Magadan oblast, in the drainage area of the Burgali River, a left tributary of the Omolon River. During 1990–1994, the Severo-Evensk Geological Exploration Expedition delineated the Burgali ore field area and covered it with surface geophysical and geochemical surveys and mining works as part of the geological prospecting program, which enabled estimating the P_2-category undiscovered resources. Further exploration activities (starting from 2009) were carried out by ZAO Omolon Gold Mining Company (OGMC), a subsidiary of PAO Polymetal Company. The financial interest in the Burgali deposit is explained by its relative proximity to the large mined Birkachan and Kubaka epithermal Au–Ag deposits (Fig. 1).

The reserves of the deposit, according to the OGMC data (2019), are 4 t gold, contained in orebodies with the average Au grades of 7.2 to 11.9 g/t, and 15 t silver (15–30 g/t). The gold resources of the deposit, estimated according to the JORC Standard, are 300–400 000 gold ounces (9–12 t gold), contained in 2–3 million tons of ores with the average Au grades of 3.5 to 5.0 g/t gold. The deposit has been mined since late 2018. The position of an orebody of the Burgali deposit (Northern zone) in the field is shown in Fig. 2.

Ore mineralogy and geochemistry were studied at the Institute of Geology of Ore Deposits, Petrography, Mineralogy, and Geochemistry, Russian Academy of Sciences (IGEM RAS) and the Northeastern Interdisciplinary Scientific Research Institute, Far East Branch, Russian Academy of Sciences (SVKNII FEB RAS) under the support of the Russian Science Foundation (project no. 14–17–00170) in 2014–2016 and a state task for IGEM RAS, starting from 2018. This paper summarizes the results of these studies.

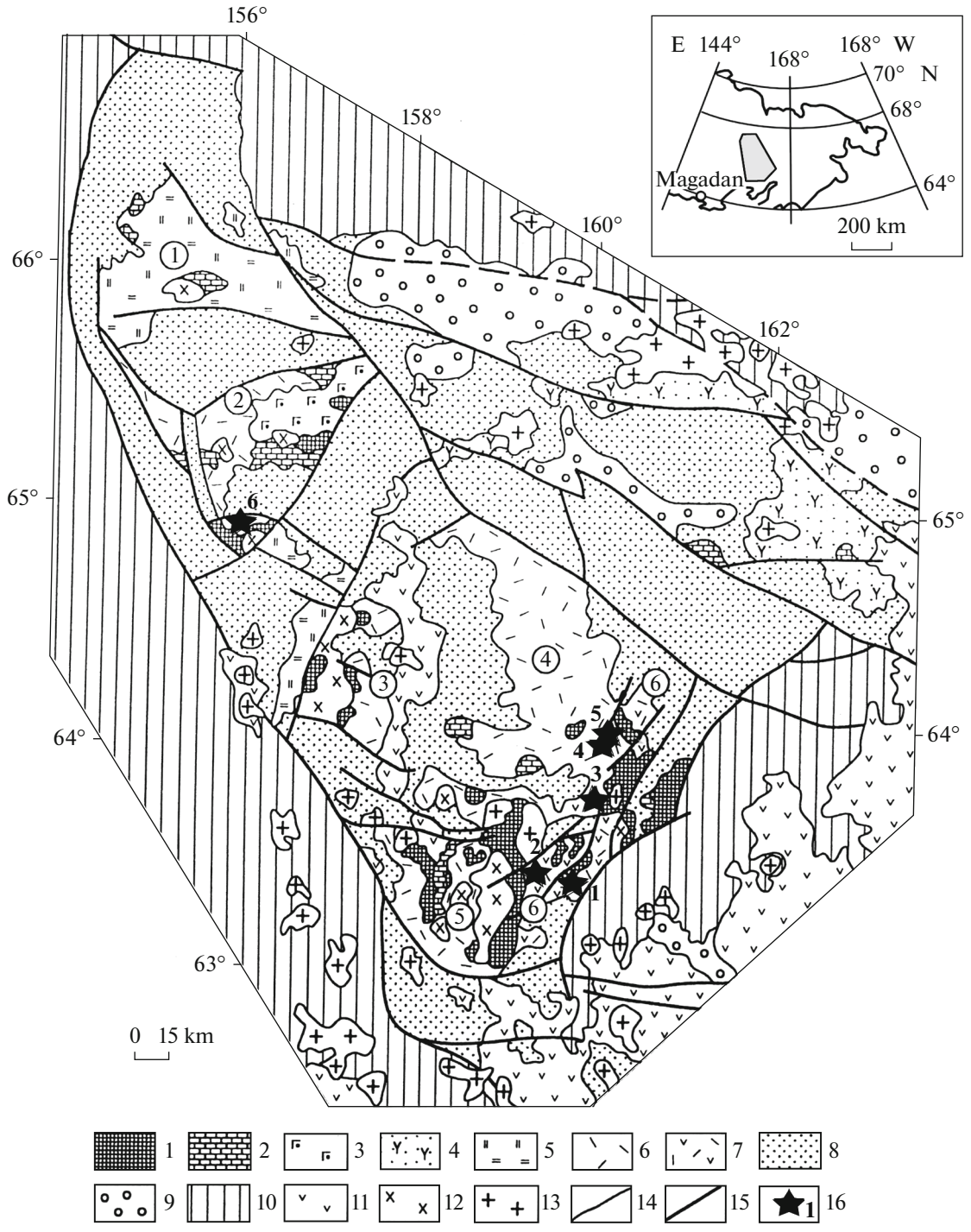

Fig. 1. Locations of gold deposits and occurrences studied within KVB in the Omolon cratonic terrane. Tectonic sketch map modified after (Gagieva, 2014). (1) Pre-Riphean basement highs; (2–9) platform cover: (2–3) lower structural unit: (2) sedimentary deposits (Riphean–Ordovician), (3) volcanosedimentary deposits (Cambrian, Vizual'naya, and Sezam formations), (4–7) middle structural unit (Devonian): (4) Namyndykan–Molandzha structural–facies zone, volcanosedimentary deposits; (5–7) Yukagir structural–facies zone, subaerial volcanics (Kedon Group): (5) trachybasaltic andesites–trachyrhyolites, (6) predominantly rhyolitic, trachyrhyolitic, and dacitic lavas, ignimbrites, and tuffs, (7) rhyolitic and trachyrhyolitic lavas, ignimbrites, and tuffs; andesites, and trachyandesites; (8–9) upper structural unit: (8) sedimentary deposits (Lower Carboniferous–Middle Jurassic), (9) sedimentary and volcanic deposits (Upper Jurassic–Lower Cretaceous); (10) structures of the folded surroundings of the cratonic terrane; (11) Cretaceous volcanics of the Okhotsk–Chukotka volcanic belt; (12–13) intrusive complexes: (12) Paleozoic, (13) Early Cretaceous; (14) geological boundaries; (15) faults; (16) epithermal Au–Ag deposits and occurrences studied. *Circled numbers:* (1–5) volcanic areas of KVB: (1) Tokur–Yuryakh; (2) Rassokha; (3) Abkit; (4) Kedon; (5) Ol'dyani–Koargychan; (6) Anmandykan volcanic zone.

Fig. 2. Burgali (Northern zone) orebody position in the field. Photograph by B.I. Ishkov.

MATERIALS AND METHODS

The section "Geological Overview" was prepared at IGEM RAS based on the archival and published data integrated with the original findings. Ore petrology and mineralogy were studied at SVKNII FEB RAS (examination of numerous polished sections under an Axioplan Imaging microscope). Ore mineral compositions were determined with a Camebax X-ray electron-probe microanalyzer equipped with an Oxford Instruments INCA add-on device (analysts E.M. Goryacheva and T.V. Subbotnikova at SVKNII FEB RAS, Magadan, and I.A. Bryzgalov at Moscow State University).

Rock-forming and some foreign element concentrations in the ores were determined by X-ray fluorescent analysis at the analytical laboratory of IGEM RAS with a PANalytical's Axios mAX sequential (wavelength–dispersive) vacuum spectrometer. The spectrometer was calibrated against industry-specific and state standard samples of the chemical compositions of rocks. The analysis was performed according to the 439-RS NSAM VIMS method, which ensures compliance of the results with the OST RF 41-08-205-04 industrial standard (analyst A.I. Yakushev). Trace element concentrations were measured with an X-Series II ICP-MS mass spectrometer with inductively coupled plasma as the ionization source (analyst Ya.V. Bychkova). Element detection limits ranged from 0.1 ng/g for heavy and intermediate elements to 1 ng, for light elements. The uncertainty of the analysis was 1–3% RPD. Gold grades of samples were determined by atomic absorption spectrometry with electrothermal atomization using a Spectr AA 22OZ spectrometer (analyst V.A. Sychkova). Geochemical indicator values were determined to study the ore formation conditions. The obtained values were tabulated and used to plot the rare-earth element (REE) and other trace element distribution curves for the ores studied.

GEOLOGICAL OVERVIEW

The Middle Paleozoic Kedon volcanic belt overlaps the Archean–Early Proterozoic basement and the Phanerozoic (pre-Devonian) sedimentary cover of the Omolon cratonic terrane (Fig. 1). The KVB consists of numerous vast fields of the Early–Middle Paleozoic felsic igneous rocks. The area covered by the Middle Paleozoic volcanics totals around 40000 km^2 (40% of the territory of the Omolon terrane). A characteristic feature of the KVB is the absence of large batholith-like intrusions (Egorov, 2004). The Kedon Complex includes the subaerial sheeted volcanic rocks of the Kedon Group and the synchronous subvolcanic and extrusive massifs; its age range spans the Devonian and the basal Early Carboniferous (Gagieva, 2014).

According to Egorov (2004), the KVB is a large (400 by 80–130 km) fragment of the Circum-Siberian marginal continental belt. However, the paleoreconstructions made by Shpikerman (1998) demonstrate that the KVB could be formed on the margin of the Omolon–Okhotsk microcontinent, which was split off from the Siberian plate. This is confirmed by the fragments of the belt which were preserved not only in the Omolon but also in the Okhotsk cratonic terrane and in the Shantar Islands (Shpikerman, 1998).

The total thickness of the volcanic sheets within the largest Kedon segment of the KVB is up to 1500–2000 m in the central part and thins down to 500–1200 m on the margins. These volcanics rest on the underlying

sequences with abrupt angular unconformity and compose homoclines with dip angles not higher than 5°–15°. The age of the volcanic rocks of the Kedon Complex was determined by the radiometric methods (Rb–Sr age is 334–377 Ma) and based on the comparatively rare fossil finds—the Givetian brachiopods and conodonts and the Famennian and Early Carboniferous conodonts and flora (Egorov and Sherstobitov, 2000).

The Kedon Group is generally characterized by the significant predominance of rhyolitic and trachyrhyolitic rocks (65–80 vol %) with subordinate dacites, trachyandesites, and trachytes (around 35%) and scarce (not more than 15%) trachybasalts and basalts (Gagieva, 2014).

In terms of petrogenic element concentrations, the basalts and trachybasalts of the Kedon Group are substantially similar to the tholeiitic basalts in the zones of rifting and intraplate magmatism, and the basaltic andesites and andesites, with the calc-alkaline basaltoids of the present-day island arcs and the Andean-type and Californian-type active continental margins (Gagieva, 2014).

The Burgali orefield consists of the stratified complex of the Middle–Late Devonian and Early Carboniferous sedimentary and volcanic rocks and the Quaternary sediments. The Middle–Late Devonian volcanic and volcanosedimentary rocks of the Kedon Group, represented by three contrasting formations, Ochakchan, Lednik, and Zakharenko (Fig. 3a), are predominant.

The *Ochakchan Formation* is composed of rhyolitic, trachyrhyolitic, rhyodacitic, and dacitic ignimbrites and tuffs with tuffaceous gravelstone and tuffstone interbeds. The thickness of this formation is up to 500 m.

The *Lednik Formation* is composed of trachyrhyodacitic and rhyodacitic ignimbrites and tuffs with tuffstone and tuffaceous gravelstone interbeds. The thickess is 0–450 m.

The *Zakharenko Formation* is composed of trachyandesitic, andesitic, basaltic-andesitic, basaltic, trachydacitic, and dacitic lavas, tuffs, and ignimbrites; the tuffs contain tuffaceous conglomerate and tuffstone interbeds. The thickness varies from 10 to 400 m.

The Upper Devonian–Lower Carboniferous sequence (Fig. 3a) is composed of tuffaceous clastic and molassoid rocks of the *Burgali Formation* (tuffaceous conglomerates, tuffaceous gravelstones, tuffstones, and tuffaceous siltstones). The thickness is estimated at 340–350 m.

Above them are the rocks of the Carboniferous System. These rocks are represented by marine carbonate and clastic sediments of the *Pushok* and *Vazhnyi formations*. Composition: conglomerates, sandstones, siltstones, marls, limestones, silty limestones, ash tuffs, and tuffites. The total thickness is 150–720 m.

The part of the sediments of the Permian Period is subordinate within the orefield. The thickness of the Quaternary eluvial and colluvial slope wash, consisting of bedrock detritus, is 1–3 m.

The intrusive and subvolcanic rocks are represented by complexes of various ages and compositions: Kedon, Middle–Late Devonian subvolcanic rocks; Bulun, Early Carboniferous intrusions (rhyolitic); Bebekan, Late Jurassic intrusions; Omolon, Early Cretaceous intrusions; and Victoria, Late Cretaceous intrusions. According to the geophysical data, the orefield is localized in the supraintrusion zone of the Early Carboniferous intrusions of the Bulun Complex, which make up a dome.

The orefield has a block structure. It is bounded by northeast trending (20°–35°) thrusts to the north and south and northwest trending (350°) high-dipping normal faults, to the east and west (Fig. 4). Inside these boundaries, there is a system of lower order cross faults (NE 40°–45° and NE 60°–65°). The gold-bearing stockwork is controlled by this fault system and the subvolcanic rhyodacites of the Kedon Group and consists of parallel en-echelon zones of extensive quartz and carbonate–quartz veining. The stockwork was confirmed over a distance of 3700 m north-northeastward (~25°) along the strike (Fig. 3b). Some veins are as thick as 1.5–2 m and as long as 300–500 m.

Three separate ore zones have been recognized within the stockwork, Burgali North, Burgali Central, and Burgali South (Fig. 3b). The lengths of the veins in the zones are 300–500 m; they vary in thickness and length and are discontinuous. Au concentrations in veins vary from 5 to 50 g/t; Ag, 5–200 g/t; and the Au/Ag ratio is around 1 : 4. The veins dip predominantly southeastward at 50°–70° and the vertical span of mineralization, according to the exploration data, is around 250 m (Fig. 4). The strike of the veins in the Southern Zone gradually turns due north, and the veins flatten downdip.

METASOMATIC ALTERATION OF HOST ROCKS

Practically all the host rocks underwent regional propylitic alteration in low-temperature carbonate–chlorite and, to a lesser extent, medium-temperature epidote–chlorite facies (Fig. 5). The sericitization and silicification zone includes numerous quartz and carbonate–quartz veins and veinlet zones that make up the northeast-trending (~25°) linear stockwork, in which ore zones and orebodies were recognized (Fig. 3b).

The deposit also contains kaolinite–quartz–illite argillizites. They occur locally in fault zones and wallrock intervals. The intensity and extent of argillization are insignificant. They usually occur in the form of lenticular formations with a thickness of several tens of centimeters (up to one meter) and a length of up to ten meters. The argillizite type wallrock metasomatites,

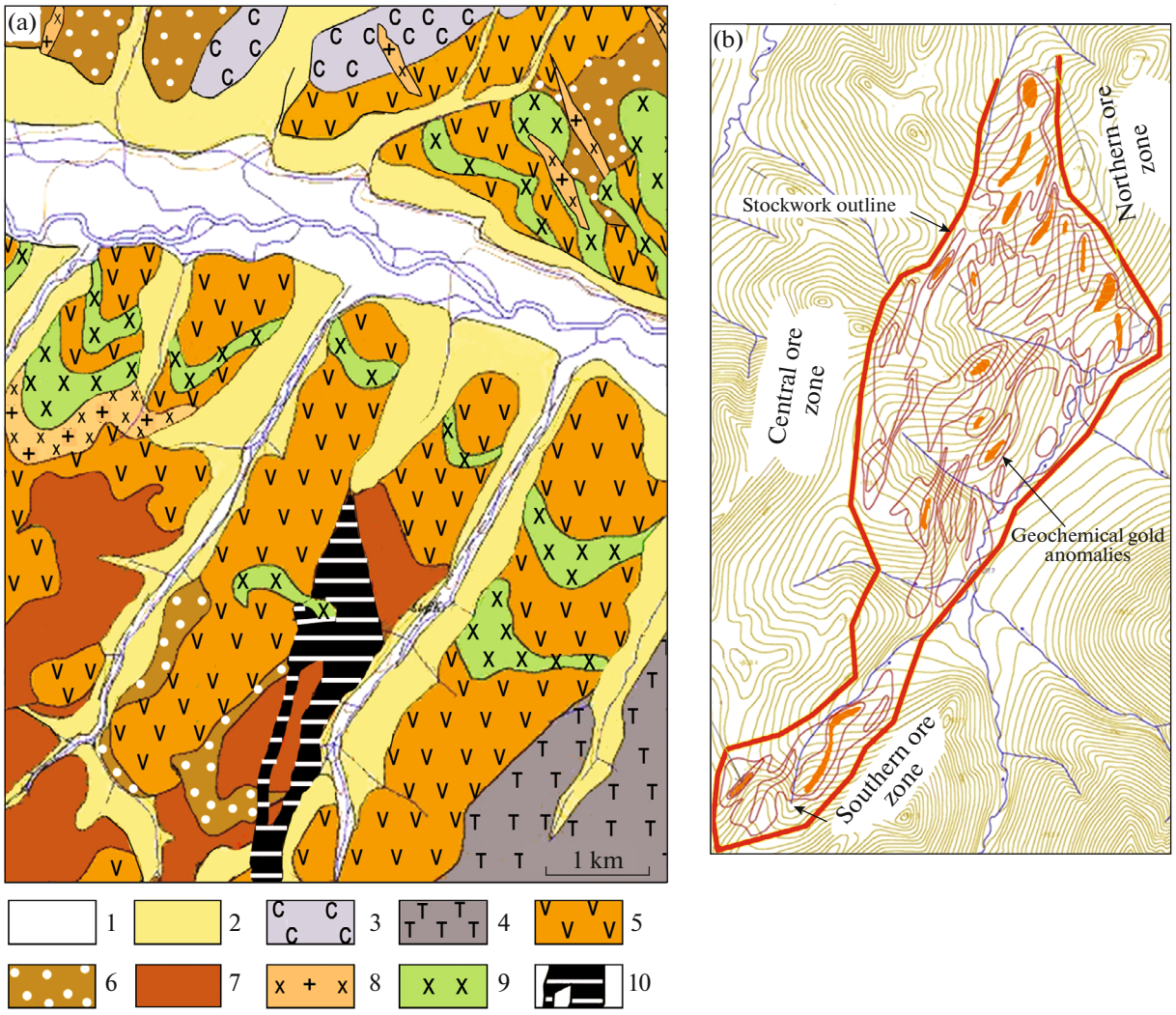

Fig. 3. Geological (a) and geochemical (b) maps of Burgali deposit after (Ishkov, 2014 r.) (1–2) Quaternary sedimentary deposits: (1) channel fill, (2) terrace deposits; (3) Carboniferous Period. Early Epoch. Tournaisian Age. Pushok Formation: limestones, siltstones, ash tuffs; (4) Devonian and Carboniferous periods. Late and Early epochs. Burgali Formation: tuffstones, tuffaceous siltstones; (5) Devonian Period. Middle and Late epochs. Zakharenko Formation: trachydacites, andesites, basaltic andesites, dacites, and ignimbrites; (6) Devonian Period. Middle and Late epochs. Lednik Formation: ignimbrites, rhyodacites, tuffstones; (7) Devonian Period. Middle and Late epochs. Ochakchan Formation: rhyolite and rhyodacite tuffs, tuffstones; (8) Bebekan complex of Late Jurassic subvolcanic intrusions: minor intrusions and dikes of porhyry syenites; (9) Bulun complex of Early Carboniferous hypabyssal intrusions: porphyry diorite laccoliths and dikes; (10) gold stockwork.

associated with ore veinlets, always contain 1–5% pyrite, which is a good ore guide. An interesting feature of this pyrite is its zoning, which accentuates the crystal habit variations in the course of crystal growth: the early pyrite is cuboctahedral, whereas the late pyrite is cubic. The lower horizons of the deposit contain widespread siderite.

The studies of the wallrock metasomatites demonstrated that the erosional truncation of the deposit is close to minimal, as indicated by the argillizites preserved on the surface.

ORE GEOCHEMISTRY

The ores of the Burgali deposit are composed predominantly of SiO_2 (89.43% on average) with appreciable concentrations of Al_2O_3 (5.87), K_2O (1.39), and Fe_2O_3 (0.84), as well as CaO (0.45) and MgO (0.24) (Table 1). Consequently, orebodies consist predominantly of quartz with subordinate adularia, carbonate, and illite. The ores are characterized by low and very low Na_2O, TiO_2, P_2O_5, and MnO concentrations (Table 1). The sulfide content in the studied ores is also very low (0.52% S_{total}) and corresponds to the very

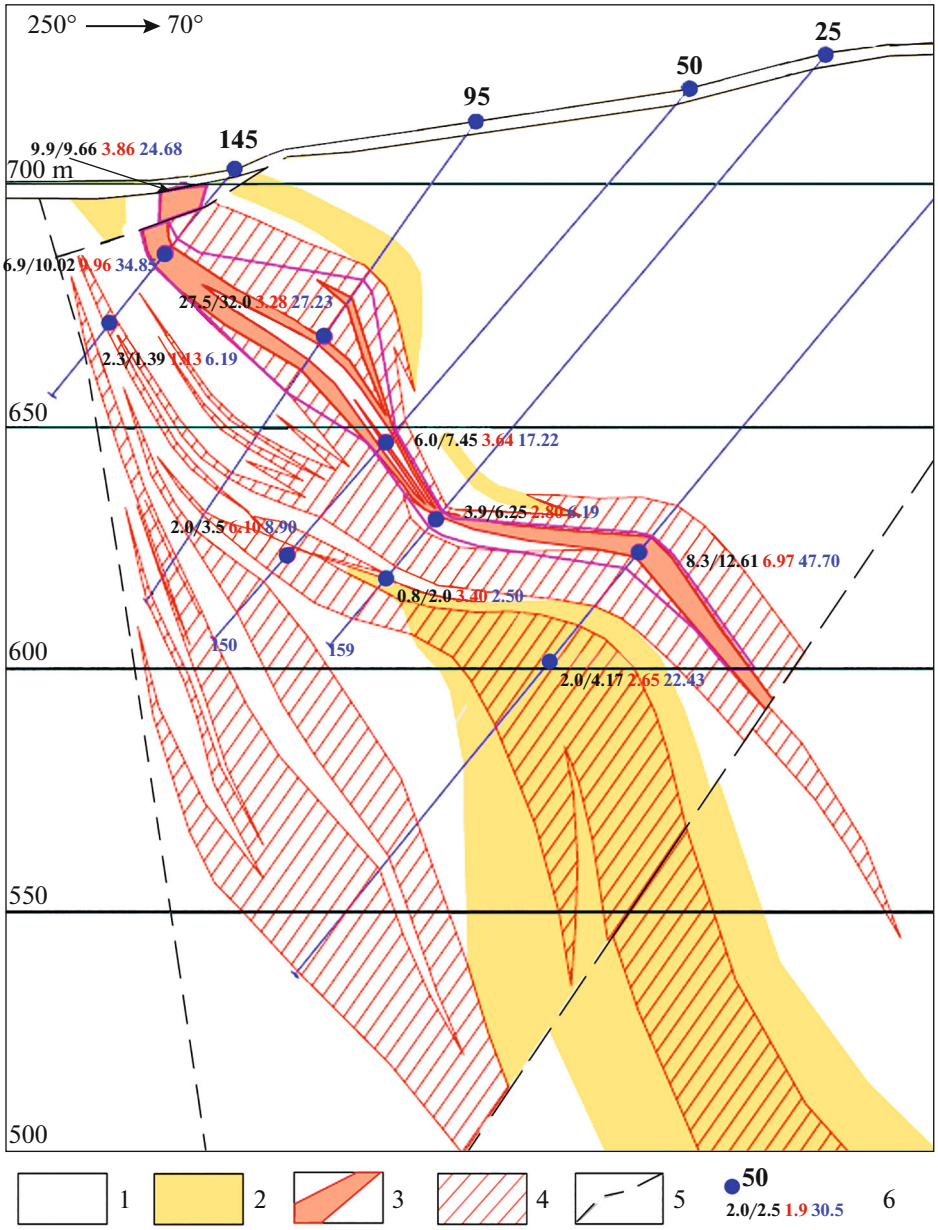

Fig. 4. Cross section along line 350 and across strike of Burgali ore zone, after (Ishkov, 2014). (1) Devonian (D_{2-3}) volcanic host rocks: andesites, dacites, andesitic and dacitic tuffs; (2) Devonian (D_{2-3}) subvolcanic rhyolites; (3) gold-bearing quartz–carbonate and quartz veins; (4) quartz–carbonate and quartz veinlet zones; (5) faults; (6) core holes: number, thickness by intersection (apparent)/horizontal thickness (m), Au and Ag grades (g/t).

low-sulfidation character of the established mineralization (see below), which is typical of the low-sulfidation epithermal Au–Ag ores of the KVB (Volkov et al., 2016).

The elemental composition analysis data for the ores of the Northern, Central, and Southern zones and host rocks of the Burgali deposit are given in Table 2 and the plot (Fig. 6), in which they are normalized to the average upper crustal values (Teilor and Mak-Lennan, 1988). The REE spectra, normalized to the average values for chondrites (Anders, 1989), are shown in Fig. 7.

The ores of the Burgali deposit are enriched in Au, Ag, As, Sb, Te, W, Mo, and Bi (Table 2, Fig. 6) as compared with their average concentrations in the upper crust (Teilor and Mak-Lennan, 1988). The enrichment factors vary from several-fold (Bi, Te) to tenfold (As, W, Mo), hundred-fold (Sb), thousand-fold (Ag), and ten-thousand-fold (Au) (Table 2, Fig. 6), providing evidence for the geochemical affinity of some trace elements and their synchronous participation in ore formation.

The REE spectra of epithermal ores are mostly chondrite-like with shallow slopes (Figs. 7a–7c),

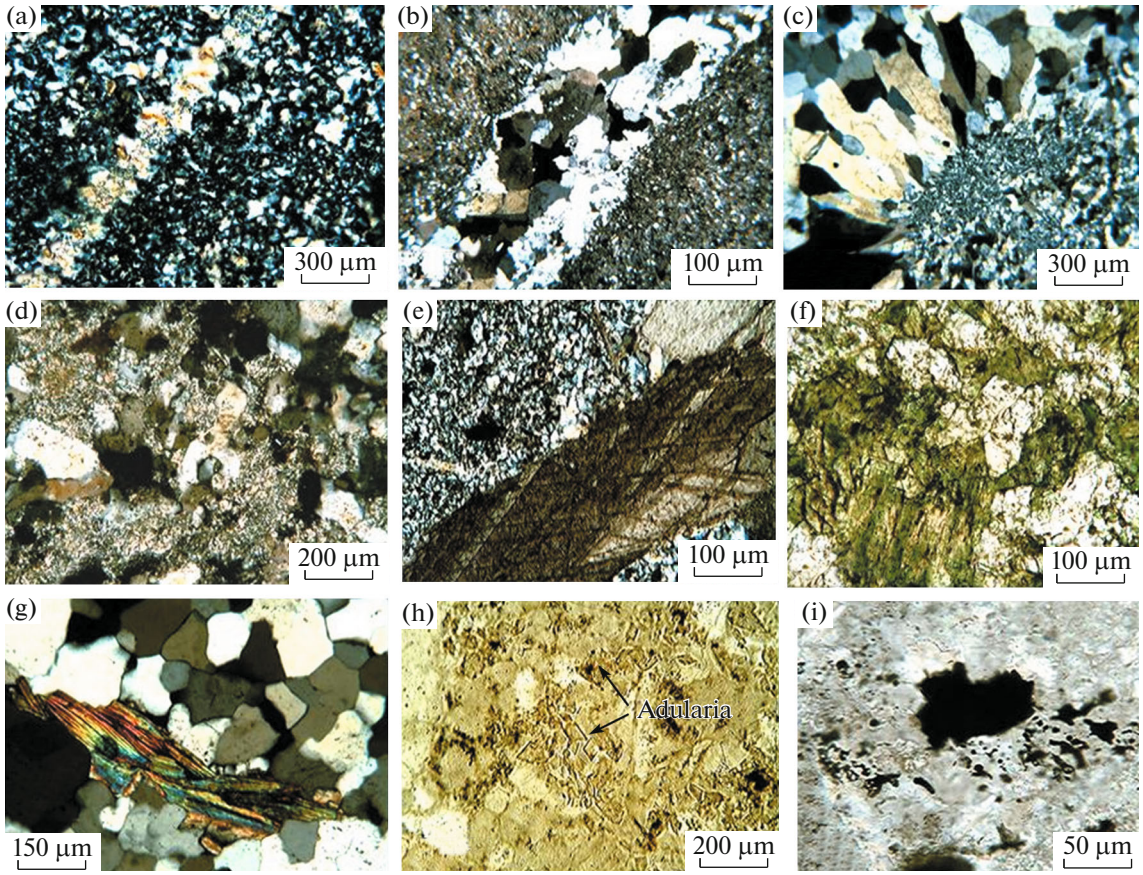

Fig. 5. Metasomatic alteration of host rocks: (a–c) silicification and late quartz veinlets in early quartz (a); (d) illitization; (e, f) carbonate veinlets (e) and carbonate–chlorite alteration (f) in non-polarized light; (g) sporadic epidotization; (h) K-feldspathization; (i) coarsely and finely disseminated ore mineralization.

largely similar in configuration with the REE spectra of the host rocks (Fig. 7d) of the Burgali deposit. The host rocks are insignificantly enriched in a fairly large number of elements (Fig. 7d).

The ores of the Central zone are characterized by chondrite-like spectral profile unlike the Southern and Northern zones (Fig. 7b). Such spectral profile is characteristic of the host andesites (Fig. 7d). A few ore samples from the Southern and Central zones display Eu peaks (Fig. 7b, 7c), also characteristic of rhyolitic tuffs (Fig. 7d).

The ores of the Northern and Southern zones displayed fairly low ΣREE values (6.78 and 13.91 g/t on average, respectively), whereas the Central zone displayed much higher values, 45.68 g/t (Table 2). The ΣREE values in ores are appreciably lower than in the host rocks (Table 2).

The Eu/Eu* values in the ores of the Burgali deposit are mostly positive and slightly exceed 1 on the average, whereas the Ce/Ce* values vary from negative to slightly positive values (from 0.06 to 1.14). Similar Eu/Eu* and Ce/Ce* combinations were also established for the host rocks (see Table 2).

ORE STRUCTURES

The veined mineralization of the Burgali deposit displays all the signatures of the near-surface genesis, which is expressed by the wide development of structures typical of epithermal deposits, namely, the colloform-banded structures consisting of quartz, chalcedony, and adularia, and less frequent brecciated, cockade, and framboidal-platy structures (Fig. 8). The illite and chalcedony bands in colloform-banded aggregates contain fine dusty ore mineral dissemination, which imparts a dark gray color to these bands (Figs. 9a, 9b). Thin section microscopy demonstrated that the late quartz veins of the deposit contain Lower Carboniferous coaly siltstone fragments (Figs. 9c–9e), filled with the timber remains (Figs. 9f–9h).

Three main groups of structures can be recognized: (1) *replacement structures*, which form as a result of the metasomatic replacement of the rocks and ores; (2) *deposition structures*, which form as a result of the various growth conditions of the mineral aggregates, free or restricted, as well as various fracture filling patterns, or veinlet formation by chalcedony deposition from viscous colloidal solutions; and (3) *cataclasis structures*

Table 1. Chemical composition of ores (in wt %) at Burgali deposit

Sample index	SiO_2	TiO_2	Al_2O_3	Fe_2O_3 total	MnO	MgO	CaO	Na_2O	K_2O	P_2O_5	S total	Σ
Burgali North												
K-250-36.8 m	91.58	<0.02	6.31	0.3	<0.01	0.16	<0.10	0.13	1.39	<0.02	0.1	99.97
K-250-37 m	91.14	0.02	6.73	0.32	<0.01	0.13	<0.10	0.1	1.43	0.02	0.08	99.97
K-250-38.2 m	87.81	<0.02	9.04	0.47	0.01	0.21	<0.10	0.11	2.06	0.02	0.11	99.84
TR1-L1-16.5	93.97	0.04	1.93	1.07	<0.01	<0.10	0.35	<0.10	0.38	0.02	2.21	99.97
TR1-L2-19.5	86.24	<0.02	6.21	0.25	<0.01	0.11	<0.10	0.1	1.29	0.02	0.1	94.32
Average	**90.15**	**0.01**	**6.04**	**0.48**	**0**	**0.12**	**0.07**	**0.09**	**1.31**	**0.02**	**0.52**	98.81
Burgali South												
YUG -1	97.23	0.01	1.73	0.37	0.053	0.12	<0.10	0.1	0.26	0.02	0.09	99.98
YUG -3	95.19	0.01	2.51	0.83	0.341	0.19	0.35	<0.10	0.46	0.02	0.08	99.98
YUG -5	94.84	0.02	1.31	1.16	0.371	0.34	1.48	0.1	0.21	0.02	0.07	99.92
YUG -7	92.15	0.08	5.06	1.06	0.016	0.24	<0.10	<0.10	1.21	0.03	0.05	99.90
K-240-QL1	95.62	0.02	1.26	1.05	0.126	0.17	0.66	<0.10	0.25	0.02	0.75	99.93
Average	**95.01**	**0.03**	**2.37**	**0.89**	**0.18**	**0.21**	**0.5**	**0.04**	**0.48**	**0.02**	**0.21**	99.94
Burgali Central												
CP182-133W, 5.4 m	85.15	<0.02	9.41	0.54	0.013	0.33	0.14	0.11	2.24	<0.02	0.24	98.17
CP2150-326 E, 11.7 m	86.78	0.11	5.85	1.56	0.038	0.31	1.27	0.11	1.3	0.04	1.2	98.57
CP2125-331E, 12.55 m	89.46	0.04	5.88	0.57	0.027	0.28	1.1	0.1	1.32	0.02	0.2	99.00
CP260-094 WK1, 34 m	81.57	0.1	9.07	0.99	0.022	0.43	1.27	0.11	2.22	0.03	2.35	98.16
CP2175-353E, 42.7 m	72.68	0.44	15.84	2.12	0.013	0.64	0.17	0.13	4.82	0.03	0.28	97.16
Average	**83.13**	**0.14**	**9.21**	**1.16**	**0.02**	**0.4**	**0.79**	**0.11**	**2.38**	**0.02**	**0.85**	98.21

X-ray fluorescence analysis, IGEM RAS laboratory, analyst A.I. Yakushev.

(insignificantly presented at the deposit), which reflect the results of destruction of the early mineral aggregates with subsequent cementation of the fragments.

ORE MINERALOGY

In terms of mineral composition, the Burgali deposit can be classified as a low-sulfidation (not more than 2% sulfides in ores) epithermal Au–Ag deposit. The ores are characterized by colloform-banded structures, finely disseminated ore mineralization, and the presence of adularia and chalcedony (Figs. 8, 9). The outlook of the most typical ore at the Burgali deposit is shown in Fig. 9a. The mineral composition of the ores is given below (Table 3).

Quartz is the most abundant gangue mineral. Two generations of this mineral have been recognized. *Quartz-I* is represented by the pale gray variety, which is intergrown with adularia and illite, making up rhythmically banded aggregates. In the course of vein formation, it was deposited first as chalcedony, which was later crystallized into the microcrystalline phase first and into columnar quartz aggregates afterwards. *Quartz-II* crosscuts the early quartz–adularia–illite aggregate as fine chalcedonic quartz veinlets (Fig. 5a).

Adularia occurs as feathery and patchy aggregates in quartz bands, has a pale cream tint, and is almost entirely replaced by clay minerals, because the samples were picked in surface mining works. Adularia concentrations in ore veins are not higher than 5%.

Illite replaces feldspar and forms independent banded aggregates in colloform structures. Due to its elevated porosity, the illite bands often contain the bulk of ore mineralization.

Clay minerals occur as pseudomorphs after adularia.

Pyrite occurs in the amount of around 3% in some parts of the veins but it was not found at all in most samples. Pyrite occurs as disseminated euhedral crystals with pentagonal and hexagonal dodecahedral habits; crystal intergrowths are less frequent. The segregations are up to 1.5 mm across. Pyrite was found to contain relics of an ovoid texture, which is typical of the transitional product of the pyrrhotite → pyrite replacement process and is referred to as the "bird's eye."

Native gold is more frequent than other minerals. It is characterized by fineness within the range of 338 to 719‰ with the average fineness of 596‰; the stan-

Table 2. Elemental composition (g/t) of analyzed epithermal ore and host rock samples from Burgali deposit

Name	ORES																		Host rocks	
	Burgali North						Burgali South						Burgali South							
sample index	k250-37	k250-36.8	k250-38.2	TR1L 116.5	TR1L 219.5	Avg	k240-QL1	YUG-1	YUG-3	YUG-5	YUG-7	Avg	CP182-133	CP2150-326	CP2125-331	CP260-094	CP2175-353	Avg	andesite	rhyolitic tuff
Au	251	145	442	0.86	848	337.46	7.0	6.1	3.5	2.2	1.5	4.06	bdl	11	18	11	2.0	8.46		
Ag	233	242	289	17	223	200.80	97	3.8	3.1	2.8	0.18	21.38	bdl	bdl	15	29	bdl	8.73	0.37	0.58
As	6.5	7.4	14	42	7.2	15.42	12	20	6.0	2.3	bdl	8.09	131	124	15	45	23	67.50	17.99	10.96
Sb	32	22	23	11	33	24.20	7.3	46	18	17	0.47	17.86	28	21	21	8.9	3.7	16.32	0.28	9.18
Cu	bdl	bdl	30	bdl	bdl	6.00	6.6	7.0	2.6	2.1	16	6.84	19	14	1.4	9.6	1.5	8.96	19.47	12.87
Pb	2.5	2.9	3.1	9.2	2.2	3.98	3.5	4.3	9.3	4.9	2.3	4.87	38	36	8.6	25	6.4	22.79	4.98	8.43
Zn	16	3.9	14	1.4	7	8.46	<0.065	7.4	3.9	5.7	4.3	4.28	17	13	6.1	12	26	14.95	92.94	3.25
Li	14	11	11	9.7	14	11.94	33	80	87	84	72	71.15	9.1	54	55	12	9.9	27.83	36.22	46.19
Be	0.67	0.69	0.48	0.22	0.51	0.51	0.51	1.5	1.1	0.50	0.34	0.79	0.61	0.96	0.68	0.97	2.2	1.09	1.01	0.66
Sc	13	16	9.5	15	11	12.90	<0.099	<0.099	<0.099	<0.099	0.73	0.15	bdl	0.45	bdl	1.1	3.2	0.94	17.55	0.86
Ti	54	14	12	146	16	48.40	14	7.0	6.2	12	303	68.45	0.38	504	128	421	2360	682.66	4197.14	564.59
V	29	21	24	22	25	24.20	19	<0.092	<0.092	<0.092	11	5.86	21	11	0.58	40	15	17.53	180.10	14.10
Cr	9.4	21	6.2	6.7	10	10.66	22	28	28	26	17	24.19	3.0	11	22	3.0	0.85	8.03	5.92	6.07
Mn	16	29	31	7.7	12	19.14	829	326	1885	2849	60	1189.67	57	238	153	121	44	122.48	1032.18	29.16
Co	0.39	0.16	0.24	3.6	0.24	0.93	6.1	4.2	10.0	12	0.90	6.56	0.68	4.7	0.61	2.1	2.1	2.05	17.08	0.59
Ni	3	2.4	1.1	0.9	0.67	1.61	2.0	2.1	2.8	2.4	1.0	2.06	bdl	0.32	bdl	bdl	bdl	0.06	5.21	0.75
Bi	1.4	2.6	5.6	0.2	1.1	2.18	0.035	<0.0004	0.34	<0.0004	0.006	0.08	0.83	0.27	0.19	0.28	0.14	0.34	0.01	0.01
Ga	3.2	2.7	4.1	0.7	2.5	2.64	4.7	3.8	2.6	8.1	15	6.83	42	43	14	10	20	25.86	13.39	5.16
Se	22	18	16	64	12	26.40	0.28	3.4	bdl	bdl	bdl	0.73	0.47	bdl	bdl	1.0	bdl	0.30	2.44	2.11
Rb	22	21	31	6.3	19	19.86	<0.027	5.5	2.2	<0.027	12	3.88	41	29	22	43	59	38.74	40.77	44.43
Sr	22	18	25	32	36	26.60	23	37	37	38	30	33.23	32	68	37	24	17	35.57	463.97	67.32
Y	0.73	0.13	0.11	24	0.27	5.05	25	2.8	11	9.1	2.4	10.02	1.5	7.5	2.1	6.1	10	5.53	15.85	3.21
Zr	3.6	0.17	0.22	5.9	0.64	2.11	<0.006	1.0	<0.006	0.15	19	4.07	1.0	45	13	27	253	67.84	89.72	29.12
Nb	bdl	bdl	bdl	bdl	bdl	0.00	<0.003	<0.003	<0.003	<0.003	1.0	0.21	bdl	2.8	0.59	2.7	13	3.86	4.31	3.48
Mo	1.3	4.3	9.9	4	2.9	4.48	4.3	10	30	32	<0.018	15.40	2.7	87	3.0	0.89	2.9	19.27	0.33	4.19
Cd	bdl	bdl	bdl	bdl	bdl	bdl	0.015	0.093	0.19	0.088	0.009	0.08	0.065	0.15	0.032	0.082	0.32	0.13	0.15	0.07
Sn	0.08	bdl	0.031	bdl	bdl	0.02	1.3	bdl	1.4	1.4	1.4	1.10	2.5	2.0	3.2	2.5	3.3	2.69	0.59	1.62
Te	5.2	11	25	0.2	5.8	9.44	0.14	bdl	bdl	bdl	bdl	0.03	2.3	0.14	1.0	0.11	bdl	0.73	0.03	0.54
Cs	0.7	1	0.9	0.4	0.7	0.74	0.54	2.1	2.1	0.54	0.57	1.16	1.3	1.3	1.6	1.4	2.5	1.62	2.94	1.26
Ba	179	171	251	277	149	205.40	426	74	157	759	1339	550.83	1120	1257	449	216	289	666.25	593.43	2900.05
La	0.43	bdl	0	4.5	0.89	1.16	0.47	0.29	0.73	1.4	5.8	1.74	0.56	16	2.6	11	17	9.44	22.81	13.63
Ce	0.77	bdl	bdl	7.7	1.6	2.01	1.1	0.60	1.9	3.0	11	3.63	0.67	31	5.1	25	35	19.45	47.76	24.50
Pr	0.05	bdl	bdl	0.93	0.15	0.23	0.17	0.089	0.36	0.45	1.2	0.46	0.10	3.6	0.60	2.6	4.3	2.23	5.96	2.67
Nd	0.4	0.084	0.07	3.7	0.77	1.00	0.94	0.57	2.1	2.1	4.1	1.94	0.40	13	2.3	9.4	16	8.16	24.36	8.23
Sm	0.062	bdl	0.007	0.83	0.085	0.20	0.64	0.31	1.4	0.82	0.64	0.77	0.12	2.3	0.35	1.6	3.1	1.49	5.09	1.19

Table 2. (Contd.)

Name	ORES																		Host rocks	
	Burgali North						Burgali South						Burgali South							
sample index	k250-37	k250-36.8	k250-38.2	TR1L 116.5	TR1L 219.5	Avg	k240-QL1	YUG-1	YUG-3	YUG-5	YUG-7	Avg	CP182-133	CP2150-326	CP2125-331	CP260-094	CP2175-353	Avg	andesite	rhyolitic tuff
Eu	0.032	0.004	0.031	0.43	0.043	0.11	0.45	0.089	0.49	0.44	0.36	0.37	0.26	0.81	0.22	0.35	0.69	0.46	1.44	1.06
Gd	0.12	bdl	bdl	1.8	0.16	0.42	2.1	0.58	2.5	1.7	0.39	1.46	0.17	2.0	0.55	1.6	2.7	1.40	5.20	1.31
Tb	bdl	bdl	bdl	0.44	bdl	0.09	0.49	0.075	0.38	0.25	0.067	0.25	0.013	0.28	0.072	0.20	0.37	0.19	0.65	0.13
Dy	0.066	bdl	bdl	3.6	0.018	0.74	3.4	0.46	2.1	1.4	0.47	1.55	0.12	1.5	0.44	1.1	2.3	1.09	3.86	0.64
Ho	bdl	bdl	bdl	0.65	bdl	0.13	0.64	0.10	0.34	0.27	0.089	0.29	0.018	0.32	0.086	0.24	0.47	0.23	0.75	0.14
Er	0.034	bdl	bdl	1.7	0.008	0.35	1.7	0.17	0.91	0.68	0.29	0.75	0.074	0.75	0.20	0.73	1.4	0.64	2.15	0.49
Tm	bdl	bdl	bdl	0.21	bdl	0.04	0.21	0.025	0.10	0.078	0.033	0.09	0.007	0.12	0.038	0.09	0.24	0.10	0.30	0.09
Yb	0.053	bdl	bdl	1.3	bdl	0.27	1.2	0.13	0.66	0.44	0.31	0.54	0.088	0.84	0.21	0.67	1.7	0.70	1.97	0.64
Lu	bdl	bdl	bdl	0.15	bdl	0.03	0.15	0.015	0.089	0.067	0.046	0.07	0.012	0.12	0.034	0.10	0.25	0.10	0.29	0.10
Hf	bdl	bdl	bdl	bdl	bdl	bdl	<0.003	<0.003	<0.003	<0.003	<0.003	<0.004	bdl	1.4	0.32	0.85	6.4	1.79	2.71	1.08
Ta	bdl	bdl	bdl	bdl	bdl	bdl	<0.001	<0.001	<0.001	<0.001	0.014	0.003	bdl	0.089	bdl	0.10	0.61	0.16	0.25	0.29
W	bdl	bdl	bdl	bdl	bdl	bdl	25	14	2.5	14	2.3	11.46	22	52	44	36	41	38.83	1.06	1.39
Tl	0.1	0.1	0.2	bdl	0.1	0.10	0.037	0.030	0.041	0.027	0.059	0.04	0.30	0.54	0.17	0.32	0.44	0.35	0.22	0.41
Th	0.1	bdl	bdl	bdl	bdl	0.02	<0.002	<0.002	<0.002	<0.002	0.94	0.19	0.094	1.9	0.38	1.7	3.2	1.45	3.57	2.73
U	0.1	bdl	0.1	3.4	0	0.72	0.42	0.032	<0.001	<0.001	0.11	0.11	0.10	0.86	0.091	0.57	1.9	0.71	0.91	0.86
∑REE	2.02	0.11	27.94	3.72	0.09	6.78	3.51	14.08	13.07	25.30	13.57	13.91	2.61	72.52	12.73	54.93	85.60	45.68	122.57	54.84
∑LREE	1.74	0.11	18.09	3.54	0.09	4.71	1.95	7.00	8.19	23.60	3.74	8.90	2.12	66.57	11.10	50.17	76.21	41.23	107.42	51.29
∑HREE	0.27	0.00	9.85	0.19	0.00	2.06	1.56	7.09	4.88	1.70	9.83	5.01	0.49	5.95	1.63	4.77	9.39	4.45	15.16	3.54
∑LREE/∑HREE	6.39	–	1.84	19.02	–	2.29	1.25	0.99	1.68	13.89	0.38	1.78	4.29	11.19	6.81	10.52	8.11	9.27	7.09	14.49
Te/Se	0.24	1.56	0.00	0.48	0.61	0.36	–	–	–	–	0.51	0.04	4.94	–	–	0.11	–	2.42	0.01	0.26
Au/Ag	1.08	1.53	0.05	3.80	0.60	1.68	1.60	1.13	0.78	8.29	0.07	0.19	–	–	1.24	0.39	–	0.97	–	–
Eu/Eu*	–	–	1.09	–	–	1.18	0.85	0.94	1.27	1.73	1.25	1.15	4.65	1.18	1.56	0.82	0.84	1.06	0.99	2.42
Ce/Ce*	0.93	–	0.86	0.97	–	0.88	0.65	0.60	0.87	1.05	0.63	0.89	0.59	1.02	1.04	1.14	1.07	1.06	1.03	0.97
∑Ce	1.65	0.07	16.83	3.41	0.08	4.41	1.55	5.08	6.94	22.60	2.64	7.76	1.74	63.51	10.53	48.22	72.40	39.28	100.89	49.03
∑Y	0.28	0.04	7.75	0.31	0.00	1.68	1.61	7.24	4.87	2.02	7.69	4.69	0.69	7.17	1.72	5.12	9.58	4.86	16.99	4.47
∑Sc	0.09	0.00	3.36	0.01	0.00	0.69	0.35	1.76	1.27	0.69	3.23	1.46	0.18	1.83	0.48	1.60	3.62	1.54	4.71	1.32

Inductively coupled plasma mass spectrometry (ICP-MS), IGEM RAS laboratory (analyst Ya.V. Bychkova). Gold concentrations in samples were determined by electrothermal atomization atomic absorption spectrometry (ETA–AAS) method on a Spectr AA220 Z spectrometer (analyst V.A. Sychkova); bdl, below detection limit. $Eu/Eu^* = Eu_N/(Sm_N^*(Tb_N^*Eu_N)^{1/2})^{1/2}$); $Ce/Ce^* = Ce_N/((2La_N + Sm_N)/3)$; REE, rare-earth elements; LREE, light REE; HREE, heavy REE.

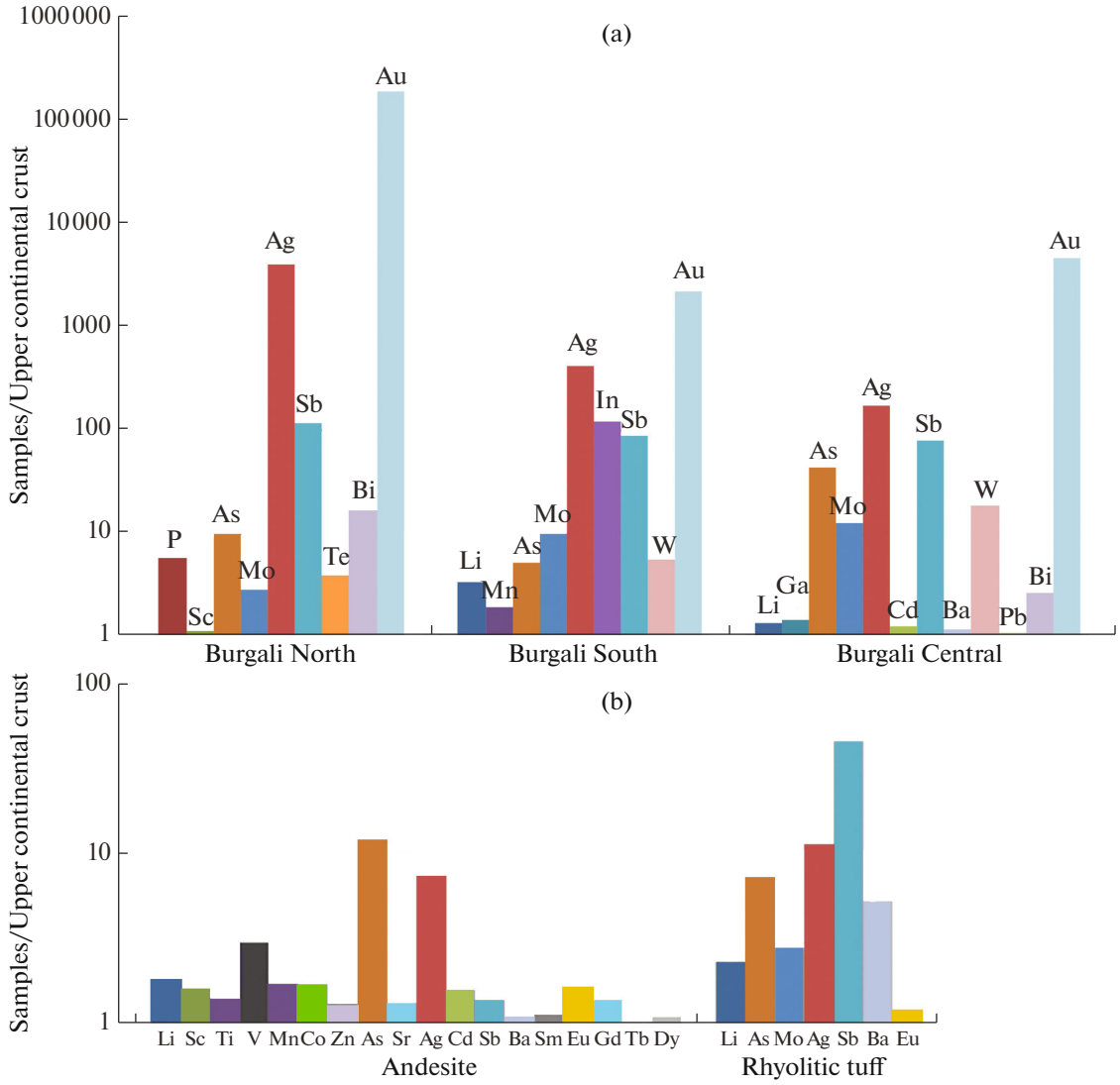

Fig. 6. Distribution of most important trace elements in epithermal ores (a) and host rocks (b) of Burgali Au–Ag deposit, normalized to average upper-crustal values (Teilor and Mak-Lennan, 1988).

dard deviation is 107; the dispersion is 11471; and most values are in the range of 600 to 650‰ (Fig. 10). The fineness distribution is polymodal. The low fineness gold from chalcedonic quartz veinlets, which is scarce, falls within a separate fineness range of 300 to 350‰.

Low fineness native gold is emplaced as free gold directly in quartz and the quartz–illite aggregate (Fig. 11). The segregations are anhedral, interstitial, bounded by the faces of the matrix's mineral crystals. The segregations can be subdivided into two size classes, fine to dusty (5–50 μm), which accounts for ~70%, and the relatively coarser material (100–300 μm), which accounts for 30%. Occasional segregations are as large as 800 μm.

Native gold with various fineness values occurs predominantly as intergrowths with polybasite and is often surrounded by a scalloped rim composed of supergene acanthite, petrovskaite, and uytenbogaardtite (Figs. 12a–12c). In addition, the Burgali deposit is characterized by gold deposition as inclusions in pyrite crystals (Fig. 12b). A certain part of the gold is deposited directly in quartz and the quartz–illite aggregate. Structural etching revealed heterogeneity within each native gold segregation. The low fineness gold segregations are surrounded by thin lower fineness rims, which provide evidence for the weakly manifested thermometamorphism during the late quartz deposition.

Native silver occurs episodically and is probably supergene, being deposited at the boundary between quartz and manganese carbonate, which is oxidized into pyrolusite. According to (Shilo et al., 1992), pyrolusite is a native silver precipitator. Native silver segregations are not larger than 200 μm.

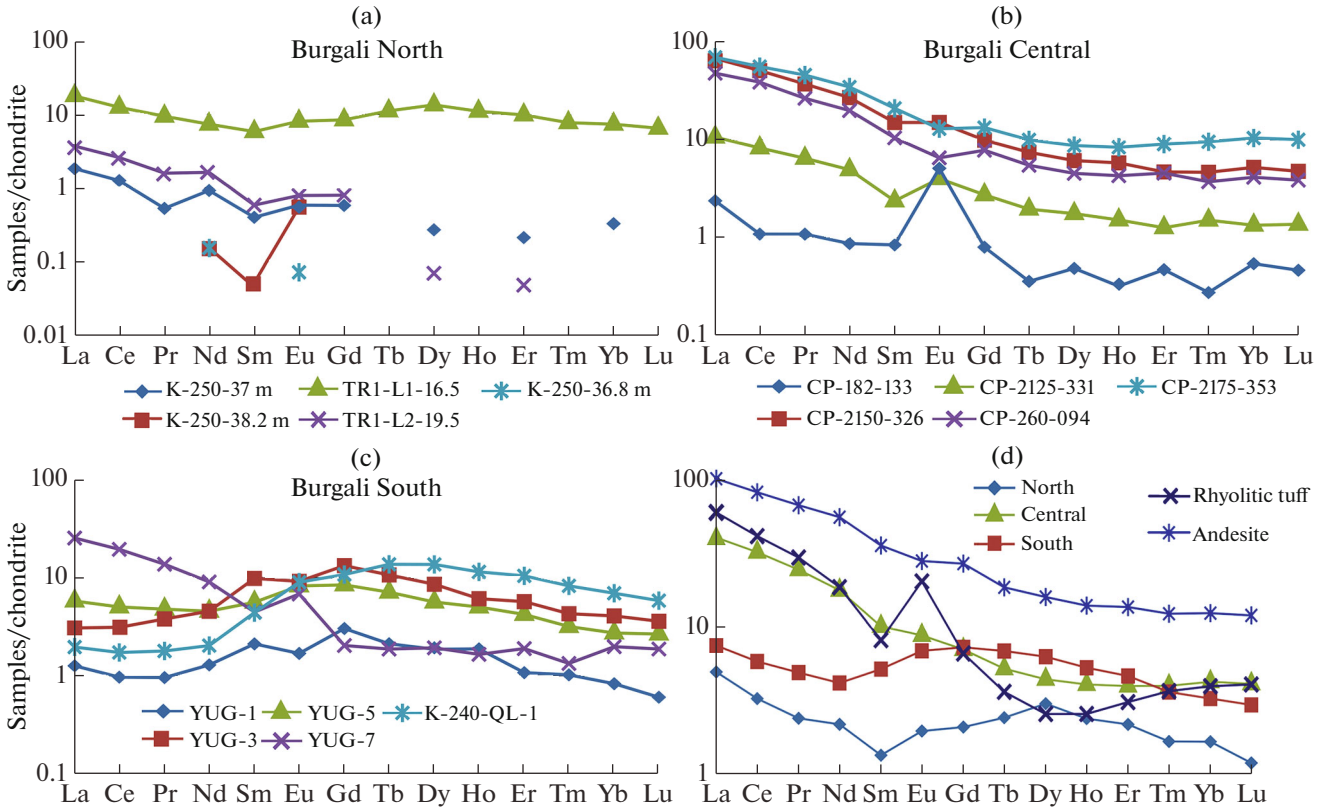

Fig. 7. Chondrite normalized (Anders, 1989) REE distribution in epithermal ores of Burgali Au–Ag deposit (a–c) and distribution of average REE values in ores and host rocks (d). See Table 2 for sample indices.

Gold-bearing pearceite $(Au,Ag)_{10}(As,Sb)S_6$ is the most abundant silver mineral in the ores (Table 4, Fig. 12d–f). It occurs as anhedral segregations and close intergrowths with native gold. The segregations are 20–500 μm in size.

Among the most important mineralogical features of the Burgali deposit is the wide development of *Au- and Te-bearing pearceite–polybasite,* in addition to the common polybasite (Fig. 13). This mineral is close to polybasite–pearceite in its optical properties, except for the slightly creamy tint. A chlorargyrite rim sometimes separates it from the low fineness gold. An intergrowth of the Au- and Te-bearing phase and a Bi mineral, the *non-stoichiometric pavonite*, was reported in one case. The axial length of the latter mineral segregations is 20–30 μm. During recalculation to the formula coefficients, the mineral displays a high deficiency in S, which is not compensated by Se.

Table 3. Mineral composition of ores at Burgali deposit broken down by abundance group

Mineral groups	Major	Minor	Rare
Gangue–metasomatic	Quartz	Kaolinite	Smectite
	Adularia	Carbonate	Zeolite
	Illite	Barite	Manganocalcite
Ore	Pyrite	Hematite	Chalcopyrite
	Polybasite–pearceite	Galena	Sphalerite
	Pearceite (Au- and Te-bearing)	Stephanite	Argyrodite
	Selenopolybasite	Acanthite	Native silver
		Native gold	Billingsleyite
		Electrum	Pavonite
Supergene	Limonite	Hydrohematite	Montmorillonite
	Pyrolusite	Uytenbogaardtite	Petrovskaite
			Chlorargyrite

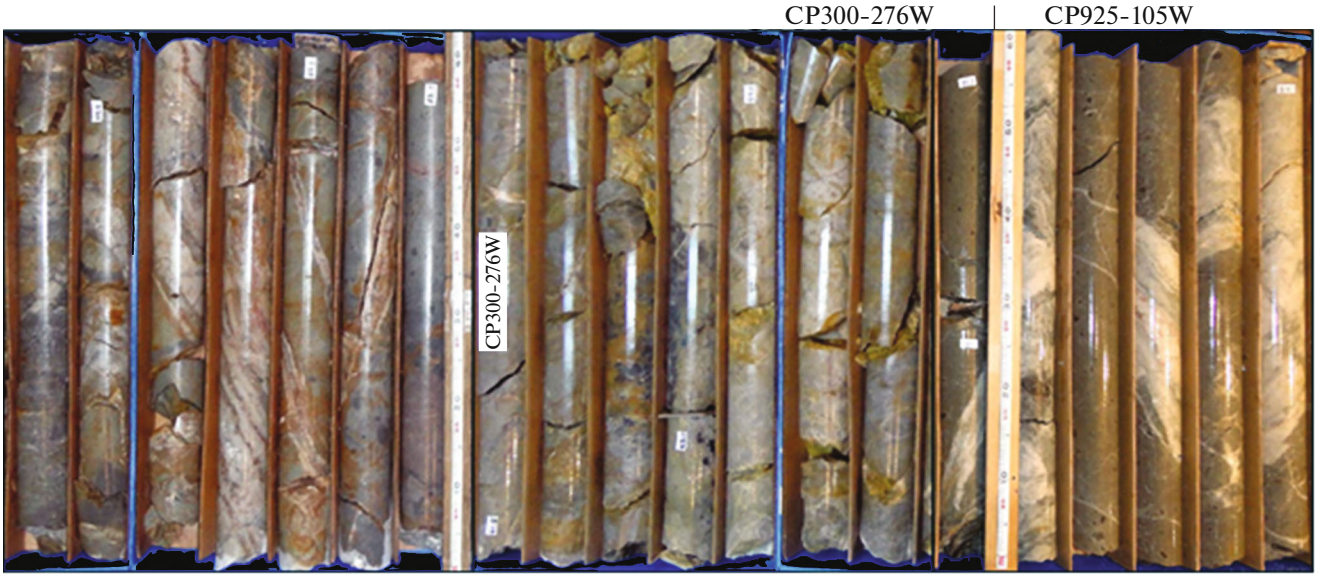

Fig. 8. Structures of ore veins at Burgali deposit (core samples from boreholes CP300-276W and CP925-105W): banded and colloform-banded, patchy and streaky with dark gray finely cavernous ore-bearing quartz.

Selenous uytenbogaardtite and petrovskaite form in the oxidized zone of the deposit (Table 5, Fig. 12). *Uytenbogaardtite* is widespread in the ores; it makes up rims up to 0.7 mm in thickness on native gold (Fig. 12a), sometimes together with chlorargyrite. Segregation morphology (rims, sometimes porous) confirms its supergene origin. The mineral is non-stoichiometric in terms of composition; some analyses correspond rather to petrovskaite (Table 5).

Stephanite occurs predominantly as independent segregations, often confined to illite clusters, and occasionally as intergrowths with native gold. Its segregations are anhedral and do not exceed 200 μm.

Acanthite occurs both as intergrowths with electrum in overgrowth rims and as independent segregations in quartz–illite vein filling material. Acanthite segregations are not larger than 100 μm.

Table 4. Gold and tellurium bearing pearceite $(Ag,Au)_{10}(As,Sb)(S,Se,Te)_6$ of Burgali deposit

Element concentrations, wt %								Formula coefficients						
S	As	Ag	Se	Sb	Te	Au	Σ	S	As	Ag	Se	Sb	Te	Au
13.51	5.73	75.72	1.27		**1.32**	**2.83**	100.4	5.77	1.05	9.62	0.22		0.14	0.34
14.22	5.68	68.42	1.44		**1.17**	**7.41**	98.35	6.19	1.06	8.85	0.25		0.13	0.88
13.05	5.13	71.35			**1.74**	**7.33**	98.61	5.83	0.98	9.47			0.2	0.87
13.12	5.76	70.79			**1.96**	**7.09**	98.71	5.83	1.09	9.35			0.22	0.84
13.56	4.82	75.85			**1.38**	**4.16**	99.77	5.88	0.89	9.78			0.15	0.49
13.03	1.79	72.24		5.46	**2.62**	**4.50**	99.65	5.81	0.34	9.58		0.64	0.29	0.53
13.50	6.27	75.21	1.28		**1.78**	**2.38**	100.4	5.75	1.14	9.53	0.22		0.19	0.28
13.02	5.02	72.35	1.42			**7.11**	98.92	5.76	0.95	9.52	0.26			0.84
13.06	5.15	71.52			**1.09**	**7.24**	98.06	5.85	0.99	9.52			0.12	0.86
13.21	4.39	70.76		1.84	**1.74**	**6.86**	98.8	5.89	0.84	9.37		0.22	0.19	0.81
12.93	4.89	69.37	1.12		**1.71**	**7.38**	97.41	5.83	0.94	9.29	0.2		0.19	0.88
12.91	4.98	69.86	1.20		**1.93**	**7.17**	98.07	5.78	0.95	9.30	0.22		0.22	0.85
12.93	3.74	70.06	1.43	2.34	**2.37**	**6.88**	99.74	5.74	0.71	9.25	0.26	0.27	0.26	0.82
14.02	4.82	74.79			**1.55**	**7.52**	102.7	5.97	0.88	9.46			0.17	0.89
13.24	4.93	72.22			**1.62**	**7.77**	99.77	5.85	0.93	9.48			0.18	0.92
15.02	5.89	69.06				**10.00**	99.97	6.43	1.08	8.79				1.19

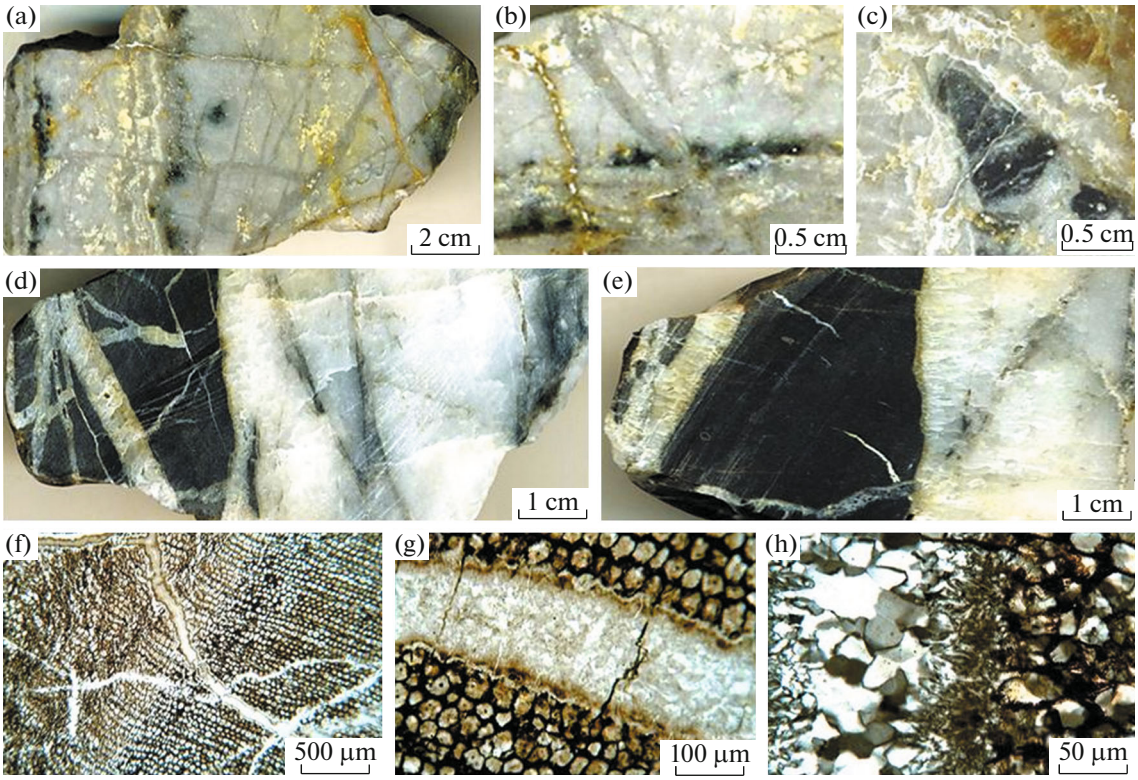

Fig. 9. Ore structures at Burgali deposit: (a) typical colloform-banded structure with occasional adularia (white) in dark concentrated ore mineralization bands; (b) veinlet: ore-rich early quartz is cross cut by late gray chalcedonic quartz veinlet; (c) brecciated structure: coaly siltstone fragments are cemented by quartz; (d, e) veinlet and brecciated structures: large coaly siltstone fragments in barren veinlets; (f–h) fragments display silicified timber texture in transmitted light images.

Selenous argyrodite can also be considered as a rare find in the Burgali ores (the Se concentration is 1.01–3.09 wt %, Table 6). Earlier argyrodite was encountered only at the Mesozoic Nyavlenga deposit (Savva, 2019), where the Au–Ag ores are combined with porphyry Mo mineralization. Other sulfides occur in very small amounts. Among them are pyrite, acanthite, galena, sphalerite, chalcopyrite, and fahlore.

RESULTS AND DISCUSSION

The problem of the age of the Au–Ag epithermal mineralization is of high metallogenic importance in the KVB. The adherents of the Paleozoic age (Stepanov and Shishakova, 1994; Kotlyar et al., 2001) believe that the Kubaka and Birkachan epithermal deposits are genetically related to the KVB and that they were formed at the Devonian–Carboniferous

Table 5. Compositions of non-stoichiometric uytenbogaardtite and petrovskaite of Burgali deposit

Element concentrations, wt %					Σ	Formula coefficients				
S	As	Ag	Se	Au		S	As	Ag	Se	Au
Uytenbogaardtite Ag_3AuS_2										
8.16		59.03	1.02	28.54	99.39	2.05		2.34	0.08	1.48
8.38		67.29	1.48	18.71	98.63	1.57		3.75	0.11	0.58
10.27		41.86	1.63	48.21	101.48	1.97		2.39	0.13	1.51
9.67		57.97	2.03	38.29	102.87	1.71		3.04	0.15	1.2
Petrovskaite AgAuS										
9.40		37.13		51.50	98.99	0.98		1.15		0.8
10.7		41.05	1.65	47.28	100.05	1.03		1.17	0.06	0.74

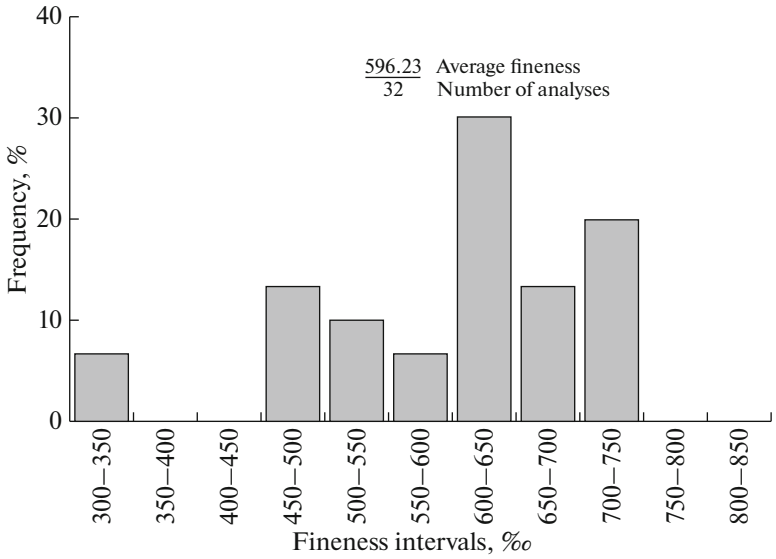

Fig. 10. Native gold fineness at Burgali deposit: occurrence frequency (%) as a function of fineness (‰).

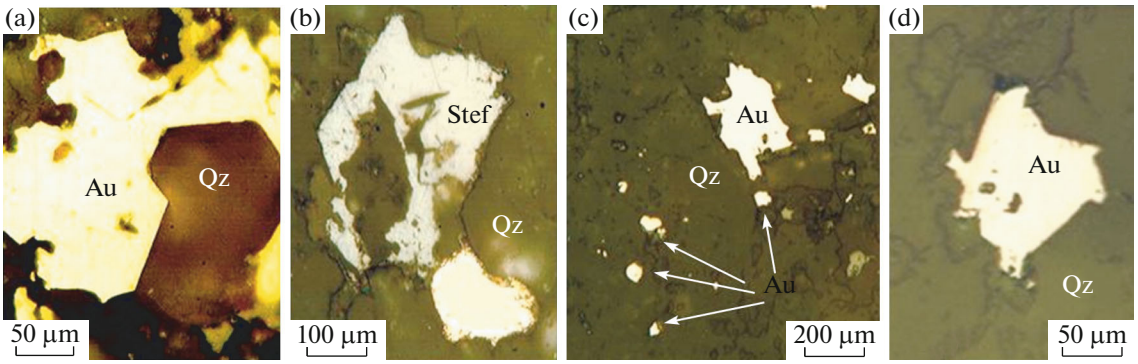

Fig. 11. Morphology of low fineness native gold segregations at Burgali deposit: (a) coarse interstitial segregation; (b) low fineness native gold intergrowth with stephanite; (c) fine dust-like segregations; (d) typical low fineness native gold segregation filling interstice between quartz crystals.

boundary (360–330 Ma). Other researchers believe that these deposits are Jurassic–Cretaceous (170–100 Ma) and their formation time coincides with the Yana–Kolyma orogeny (Natalenko et al., 2002). During this period the folded structures of the clastic–carbonate Verkhoyansk Complex (C–J) were thrust onto (overrode) the structures of the Omolon fragment of the KVB.

According to (Akinin et al., 2020), ore mineralization in the Tsokol'naya zone of the Kubaka deposit is sandwiched (in terms of formation time) between the eruptions of the ore-bearing Late Devonian volcanics of the Kedon Group (U–Pb zircon age of ca. 370 ± 2.5 Ma, SHRIMP) and the post-ore crosscutting Early–Middle Jurassic trachybasalt and picrobasalt dike of the Omolon Complex (with a 40Ar/39Ar plateau age of 179 ± 8 Ma), which does not penetrate the Carboniferous Korbin Formation. Data obtained by these authors indicate the Carboniferous upper age limit of the epithermal gold mineralization with a high degree of certainty (Akinin et al., 2020).

Fragments of the Lower Carboniferous coaly siltstones were for the first time recognized in the late quartz veinlets at the Burgali deposit (Figs. 9c–9e). They represent fragments of coalified timber with the distinctly visible cellular structure, cemented with quartz (Figs. 9f–9h). This fact allows us to estimate the age of mineralization at the Burgali deposit as Carboniferous and does not contradict the latest data on the age of the Kubaka deposit (Akinin et al., 2020).

Comparative analysis (Table 7) demonstrated a great similarity in the geological structure, orebody morphology, and ore composition between the Burgali deposit and other epithermal low-sulfidation Au–Ag deposits in the KVB.

As a result of the increase in pressure, light REE migrate into the aquatic fluid, whereas heavy REE are

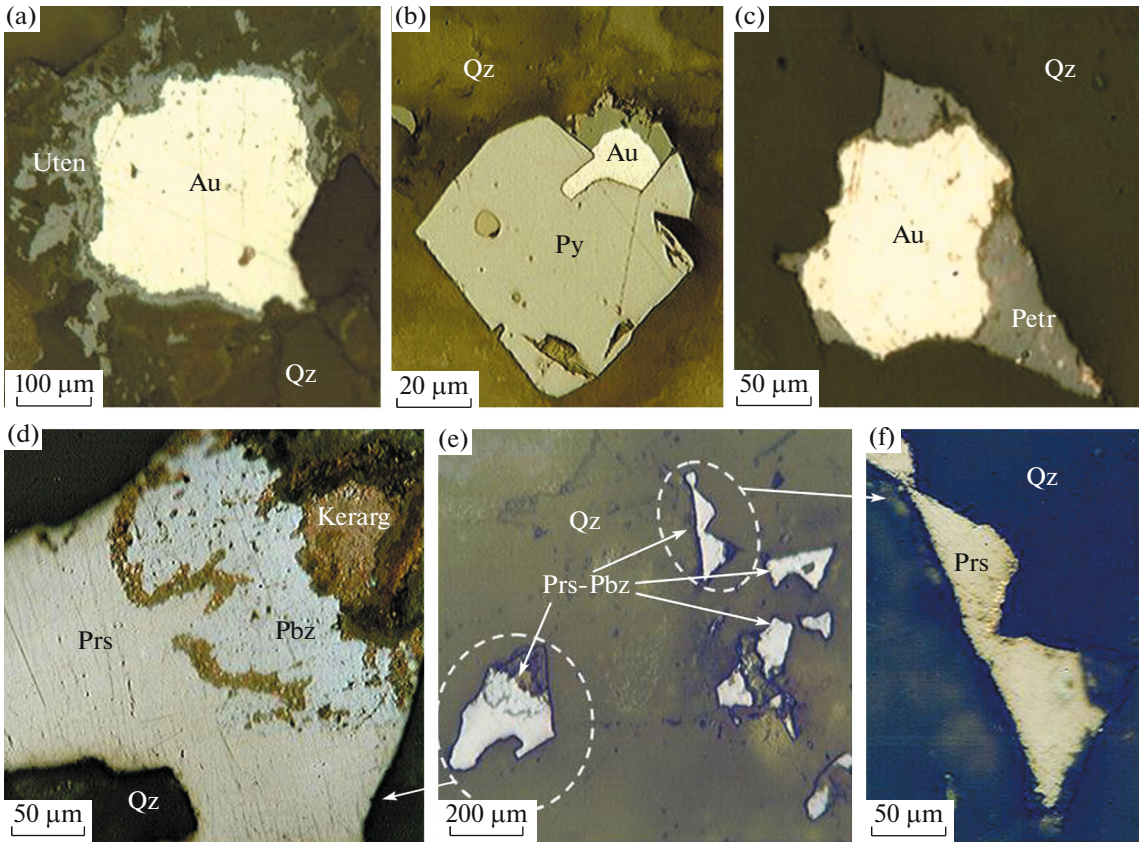

Fig. 12. Typical intergrowths of ore minerals at Burgali deposit: (a) uytenbogaardtite rim on native gold segregation; (b) pyrite intergrowth with native gold; (c) petrovskaite formation on periphery of native gold segregation; (d) gold-bearing pearceite intergrowth with polybasite and supergene cerargyrite; (e, f) gold-bearing pearceite–polybasite.

retained in the magma, which allows us to classify the former as "hydrophile" and the latter as "magmaphile" elements (Zharikov et al., 1999). In addition, REE were divided into three groups: ceric (La, Ce, Pr, Nd), yttric (Sm, Eu, Gd, Dy, Ho), and scandic (Er, Yb, Lu) (Mineev, 1974). Therefore, Table 2 demonstrates that the REE spectra of the ores and host rocks studied are dominated by light hydrophile lanthanides of the ceric group.

The Eu and Ce anomalies are usually considered as the markers of the oxidation–reduction potential of the ore formation environment (Bortnikov et al., 2007; Goryachev et al., 2008; Jones and Manning, 1994). The ores of the Burgali deposit are characterized by mostly positive Eu/Eu* values, whereas the Ce/Ce* values vary from negative to slightly positive values (see Table 2). This combination of Eu/Eu* and Ce/Ce* ratios indicates the existence of oxidizing conditions during the deposition of the epithermal ores of the deposit (Jones and Manning, 1994).

The distribution pattern and the profiles of the REE spectra (Fig. 7) as well as the combination of the Eu/Eu* and Ce/Ce* ratios (see Table 2) of the studied ores are largely similar to those of the host rocks of the deposit. These facts enable us to conclude that the host volcanics and andesitic magmas are the most probable sources of ore material for the ore-forming fluids.

The comparative analysis of the average concentrations of trace elements and REE in the ores of the Kubaka, Birkachan, and Burgali Au–Ag deposits in the KVB demonstrates an almost complete analogy in the composition and distribution spectra, which indicates the similarity in the ore formation conditions between these ore deposits (Volkov et al., 2016). We note the appreciable difference in the trace element compositions of the ores in the Northern, Central, and Southern vein zones of the Burgali deposit (see Fig. 6), which is attributable to their different erosional truncation level.

The comparison of the obtained data with the known published examples (Vinokurov et al., 1999; Kravtsova, 2010; Volkov et al., 2018) suggests that the established ore characteristics, i.e., the depletion of rare earth elements, prevalence of light lanthanides over heavy lanthanides, and the positive europium anomalies, are typical of the epithermal ore formation system.

Our study demonstrates that the ores of the Burgali deposit can be classified as very low-sulfidation (0.5–

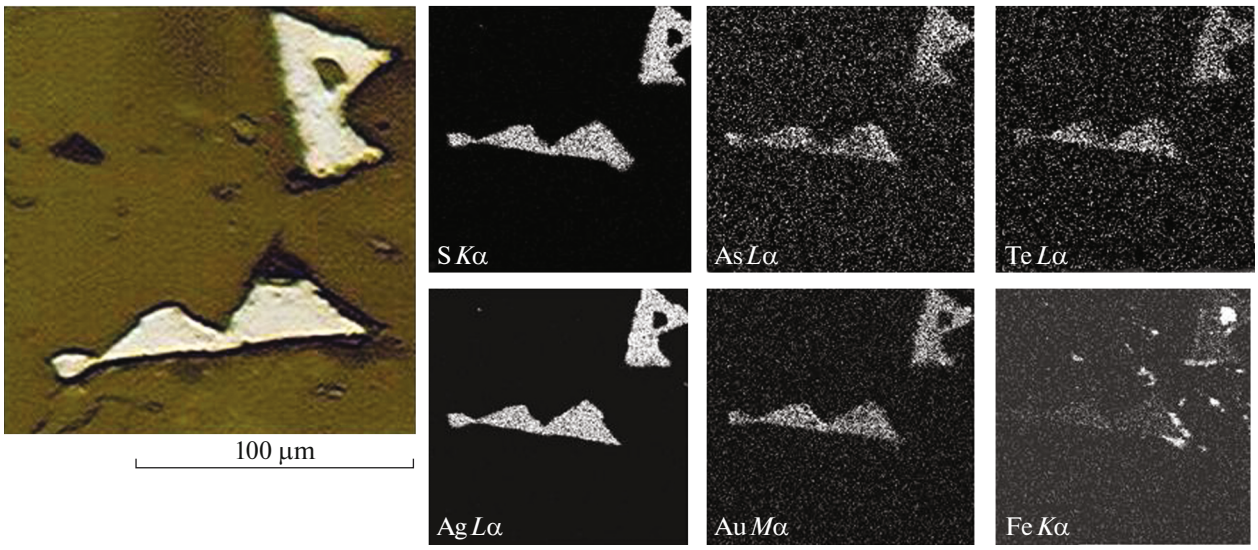

Fig. 13. Even Au, Ag, and Te distribution in gold-bearing pearceite (images in characteristic X-rays).

2%), which is typical of the Kubaka and Birkachan epithermal low-sulfidation Au–Ag deposits (Table 7). The low sulfidation makes the ores of the deposit easy for concentration, including heap leaching.

Among the main mineralogical features of the ores of the Burgali deposit is the wide occurrence of the Au- and Te-bearing pearceite–polybasite $(Ag,Cu)_{16}(As,Sb)_2(S,Se)_n$. The compositions of the minerals of this series are characterized by isomorphous substitutions of Sb by As, Ag by Cu, and S by Se. The tellurium concentration in polybasite at the Burgali deposit varies from 0.00 to 2.62 wt %, and the Au concentration, from 2.38 to 10.00 wt % (most frequently, 6–7 wt %); the mineral is essentially arsenical, whereas Cu is absent altogether (Table 4). During the recalculation in the formula coefficients, polybasite displays a high deficiency in S, which is not compensated by Se (Table 4). Among the epithermal deposits of northeastern Russia, the Au-bearing polybasite was encountered in the ores of the Mesozoic Kupol, Dal'nee, and Sopka Kvartsevaya deposits (Savva, 2019). It was also encountered in the ores of the Pallancata epithermal Au–Ag deposit (Peru) (Jorge et al., 2013).

It should be noted that the polybasite–pearceite group is characterized by a wide isomorphous miscibility between Sb and As. The group includes not only polybasite and pearceite but also stephanite and billingsleyite. Moreover, the monoclinic polytypes Tac, 2Tac, and T2a2c were also described for the natural phases with compositions close to those of polybasite–pearceite (Yushko-Zakharova et al., 1986). Based on the results of the thermodynamic analysis of the phase relations, Nekrasov (1991) demonstrated the possibility of the existence of intermediate aurostibite in the Au–Ag–Sb–S system and petzite, in the Au–Ag–Te system with their subsequent integration into complex compounds for the ores of epithermal silver sulfosalt deposits.

The presence of Se and Te in polybasites was reported earlier. For instance, Oreshin (1979) calculated the formula $(Ag, Cu)_{15}$ $(Sb, As)_2$ $(S, Se, Te)_{15}$ for the selenous polybasite and referred Se and Te to S. The gold-bearing phase, which we termed as Au- and Te-bearing pearceite, is adequately calculated in 17 formula units and takes the form $(Ag,Au)_{10}$ (As, Sb) $(S, Se, Te)_6$ as a phase intermediate between polybasite and billingsleyite (based on S) with stable Au concentrations of 6 to 7 wt %. This complex mineral phase is presumably formed under nonequilibrium, steep-gradient conditions. The presence of polytypes in the polybasite–pearceite group complicates identifying such compositions from the X-ray structural analysis data.

Also unusual is the presence of selenous argyrodite with 15.82–15.86 wt % S, 1.01–3.09 wt % Se, 5.53–6.89 wt % Ge, and 73.92–76.23 wt % Ag in the ores (Table 6). Earlier, argyrodite was encountered only in the Mesozoic deposit Nyavlenga, where epithermal Au–Ag ore is combined with porphyry Mo mineralization (Savva, 2019). According to the ICP-MS data, the ores of the Burgali deposit are also characterized by elevated Mo concentrations (Fig. 6).

CONCLUSIONS

Based on the results of the comparative analysis, a similarity in geological structure, orebody morphology, and ore composition was established between the Burgali deposit and other epithermal low-sulfidation Au–Ag deposits in the KVB.

Table 6. Compositions of ore minerals of Burgali deposit, wt %

Element concentrations, wt %							Formula coefficients					
S	As	Ag	Se	Sb	Ge	Σ	S	As	Ag	Se	Sb	Ge
Argyrodite Ag_8GeS_6												
15.82		73.92	3.09		5.53	98.36	5.71		7.95	0.46		0.88
15.36		76.23	1.01		6.89	99.49	5.56		8.20	0.15		1.10
Acanthite Ag_2S												
12.52		85.60				98.12	0.99		2.011			
10.32		83.53	0.61			97.01	0.87		2.104	0.02		
Pyrite FeS_2												
S	Fe	As	Se	Pb	Zn		S	Fe	As	Se	Pb	Zn
53.18	46.65					99.83	2.00	1.005				
53.68	46.74					100.42	2.00	1.000				
53.77	46.68					100.45	2.00	0.998				
53.74	47.04					100.78	2.00	1.003				
52.71	45.81				0.74	99.26	2.00	0.999				0.14
54.07	47.07					101.14	2.00	1.000				
54.13	47.14					101.27	2.00	1.000				
53.55	46.97					100.52	2.00	1.005				
53.62	46.77					100.4	2.00	1.001				
53.32	47.02					100.34	1.99	1.008				
52.22	46.25	1.13				99.60	1.99	1.011	0.02			
Galena PbS												
S	Fe	Cu	Se	Pb	Zn	Σ	S	Fe	Cu	Se	Pb	Zn
12.87	0.96		0.78	84.55		99.14	0.96	0.041		0.02	0.976	
12.79	1.98		0.67	84.79		99.56	0.94	0.083		0.02	0.961	
12.22				85.28		98.17	0.96			0	1.038	
12.7			0.91	86.73		100.34	0.96			0.03	1.013	
12.95			0.76	85.43		99.15	0.98			0.02	0.999	
Sphalerite ZnS												
33.00	2.93				63.11	99.04	1.01	0.051				0.943
33.20	2.15				63.56	100.02	1.01	0.038				0.95
Chalcopyrite $CuFeS_2$												
35.08	31.49	33.51				100.80	2	1.032	0.965			
36.00	31.19	33.40				100.59	2.04	1.012	0.953			
Fahlore $(Ag, Cu)_{10}(Zn, Fe)_2(As, Sb)_4S_{13}$												
S	Fe	Cu	Zn	As	Ag	Sb	Σ	S	Fe	Cu	Zn	As	Ag	Sb
26.53	1.90	39.50	6.52	9.77	1.23	14.72	100.2	13.0	0.54	9.77	1.57	2.05	0.18	1.90
26.34	2.62	39.11	6.17	11.12		12.78	98.14	13.0	0.74	9.75	1.49	2.35		1.66
Pavonite (based on sulfur) $AgBi_3S_5$? (non-stoichiometric; recalculated approximately to $Ag_3Bi_2(Se, Se)_5$														
S	Fe	Au	Se	Bi	Ag	Sb	Σ	S	Fe	Au	Se	Bi	Ag	Sb
15.40			0.72	50.55	32.34		99.01	4.19			0.08	2.11	2.62	
15.41			0.71	50.09	32.32		98.55	4.20			0.08	2.10	2.62	

Table 7. Comparative geological–mineralogical characteristics of Burgali, Birkachan, and Kubaka deposits

Burgali	Birkachan	Kubaka
Host rock composition and age		
(1) D_{2-3} zh. ld. oc (Zakharenko, Lednik, and Ochakchan formations), andesites and dacitic andesites; D_{2-3} kd, subvolcanic rhyodacite bodies; (2) D_3– C_1 br, siltstones of Burgali Formation	(1) D_{2-3} grt (Gruntovoi Formation), dacitic andesites; (2) D_3, subvolcanic dacite bodies; (3) C_1krb (Korbin Formation), tuffs and coaly siltstones	(1) D_{2-3} kd (Kedon Formation), andesites and andesitic tuffs; (2) C_1krb (Korbin Formation), tuffs and coaly siltstones
Orebody morphology		
Vein and veinlet zones. Northeastward strike (azimuth ~25°); thickness 20–0.2 cm; length 3.5 km	Vein and veinlet zones. Strike azimuth 60°–65°; thickness, 10–0.1 cm; length, 0.6 km	Veins and stockwork zones. Strike azimuth 35°–45°; thickness, 1–3 m; vein swells, up to 20 m; length, 0.8 km
Structures		
Predominantly colloform-banded, sometimes brecciated	Predominantly colloform-banded, sometimes brecciated	Predominantly brecciated and cockade, intricately combined with colloform-banded and framboidal–platy structures
Major gangue mineral percentages		
Quartz, chalcedony, 70 Adularia, 3–5 Illite, 15	Quartz, chalcedony, 80 Adularia, 10 Illite, 5 Dickite, 5	Quartz, chalcedony, 50 Adularia, 15 Illite, 5 Carbonate, 30 Fluorite, 5
Major ore mineral percentages		
Native gold, 85 Pyrite, 5 Polybasite, 10	Native gold, 85 Pyrite, marcasite, 10 Ag-tetrahedrite, 5	Native gold, 85 Chalcopyrite, 5 Hematite, 15
Exotic minerals		
Au- and Te-bearing pearceite, argyrodite, pavonite, petrovskaite, uytenbogaardtite	Hessite, altaite, cubanite, luzonite	Native Fe, Sn, Cu; stistaite, graphite, uytenbogaardtite
Fineness, ‰		
350–750	450–800	250–750
Ore sulfidation, %		
0.5–2	0.1–1.5	0.1–0.5

The ores of the deposit have very low-sulfidation with finely disseminated mineralization and widespread chalcedony. The structures are predominantly colloform-banded and often combined with the brecciated structures. The late quartz veins contain fragments of coaly siltstones (C_1), filled with remains of timber fragments, which indicate the Carboniferous age of the ore mineralization. Among the most important mineralogical features, in our opinion, is the broad development of the Au- and Te-bearing pearceite–polybasite in the ores.

The ores' geochemistry agrees well with the mineral composition. The ores are enriched in a fairly narrow range of elements (Au, Ag, As, Sb, Te, W, Mo, and Bi) and characterized by a small sum of REEs. The presence of positive Eu-anomalies was noted. The REE spectra are dominated by light hydrophile lanthanides of the ceric group. The ores are abnormally poor in REEs; in addition, the light lanthanides prevail over the heavy ones. The established combinations of the Eu/Eu* and Ce/Ce* ratios indicate the oxidizing ore formation environment.

The outlook for Au and Ag reserve additions at the Burgali deposit depends on the further studies and exploration of the ore-bearing stockwork.

The data given in this paper are practically important for regional metallogenic forecasts and for the prospecting and evaluation of epithermal Au–Ag deposits.

ACKNOWLEDGMENTS

We thank the management and geologists of the Omolon Gold Mining Company and the Magadan Office of PAO Polymetal for their assistance in our studies.

FUNDING

This study was supported by a state assignment for the Institute of Geology of Ore Deposits, Petrography, Mineralogy, and Geochemistry, Russian Academy of Sciences (project "Metallogeny of Mining Districts within the Volcano–Plutonogenic and Folded Orogenic Belts of Northeastern Russia").

CONFLICT OF INTEREST

The authors declare that they have no conflict of interest.

REFERENCES

Akinin, V.V., Glukhov, A.N., Polzunenkov, G.O., Al'shevskii, A.V., and Alekseev, D.I., The age of the Kubaka epithermal gold–silver deposit (Omolon Massif, Northeast Russia): geological and isotopic–geochronological constrains (U–Pb and $^{40}Ar/^{39}Ar$ Methods), *Russ. J. Pac. Geol.,* 2020, vol. 14, no. 1, pp. 32–42.

Anders, E., Abundances of the elements: meteoric and solar, *Geochim. Cosmochim. Acta,* 1989, vol. 53, pp. 197–214.

Bortnikov, N.S., Gamyanin, G.N., Vikentyeva, O.V., Prokof'ev, V.Yu., Alpatov, V.A., and Bakharev, A.G., Fluid composition and origin in the hydrothermal system of the Nezhdaninsky Gold Deposit, Sakha (Yakutia), Russia, *Geol. Ore Deposits,* 2007, vol. 49, no. 2, pp. 87–128.

Egorov, V.N., Structure, Magmatism, and Metallogeny of the Middle Paleozoic of the southern Omoln massif, *Extended Abstract of Candidate (Geol.–Min.) Dissertation,* Magadan: SVKNII DVO RAN, 2004.

Egorov, V.N., and Sherstobitov, P.A., Caledonian volcanoplutonic association of the southeastern Omolon massif, *Magmatizm i metamorfizm Severo-Vostoka Azii. Materialy IV regional'nogo petrograficheskogo soveshchaniya po Severovostoku Rossii* (Magmatism and Metamorphism of Northeast Asia. Proc. 4th Regional Petrographic Conference on Northeast Russia), Magadan: Kn. Izd-vo, 2000, pp. 23–29.

Gagieva, A.M., Middle Paleozoic volcanism of the Omolon massif (northeast Asia): chemical composition and problems of geodynamic interpretation, *Vestn. ONZ RAN,* 2014, vol. 6, pp. 1–12.

Goryachev, N.A., Vikent'eva, O.V., Bortnikov, N.S., Prokof'ev, V.Yu., and Alpatov V.A., The world–class Natalka gold deposit, Northeast Russia: REE patterns, fluid inclusions, stable oxygen isotopes, and formation conditions of ore, *Geol. Ore Deposits,* 2008, vol. 50, no. 5, pp. 362–390.

Jorge, E., Gammara, U., and Ricardo, C., Preliminary mineralogy and ore petrology of the intermediate-sulfidation Pallancata deposit, Ayacucho, Peru, *Can. Mineral.,* 2013, vol. 51, pp. 67–91.

Kotlyar I.N., Zhulanova I.L., Rusakova T.B., and Gagieva A.M. *Izotopnye sistemy magmaticheskikh i metamorficheskikh kompleksov Severo-Vostoka Rossii* (Isotope Systems of Magmatic and Metamorphic Complexes of Northeast Russia), Magadan: SVKNII DVO RAN, 2001.

Kravtsova, R.G., *Geokhimiya i usloviya formirovaniya zolotoserebryanykh rudoobrazuyushchikh sistem Severnogo Priokhot'ya* (Geochemistry and Conditions of Formation of Gold–Silver Ore-Forming Systems of the Northern Okhotsk Region), Novosibirsk: *GEO*, 2010.

Manning, D.A.C., Comparison of geochemical indices used for the interpretation of palaeoredox conditions in ancient mudstones, *Chem. Geol.,* 1994, vol. 111, pp. 111–129.

Mineev, D.A., *Lantanoidy v rudakh redkozemel'nykh i kompleksnykh mestorozhdenii* (Lanthanides in Ores of the Rare-Earth and Complex Deposits), Moscow: Nauka, 1974.

Natalenko, M.V., Struzhkov, S.F., Ryzhov, A.B. Vakin, M.E., Politov, V.K., Ishkov, B.I., Gilles, B., Karchavets, V.P., Ustinov, V.I., and Shergina, Yu.P., Geological structure and mineralogy of ores of the Birkachan deposit, Magadan district, *Rudy Met.,* 2002, no. 6, pp. 37–52.

Nekrasov, I.Ya., *Geokhimiya, mineralogiya i genezis zolotorudnykh mestorozhdenii* (Geochemistry, Mineralogy, and Genesis of Gold Deposits), Moscow: Nauka, 1991.

Oreshin, V.Yu., S.M. Sandomirskaya, S.M., and Chuvikina, N.G., Selenium polybasite in ores of the Neogene gold–silver deposit, *Mineralogiya serebra blizpoverkhnostnykh mestorozhdenii* (Silver Mineralogy of Subsurface Deposits), *Tr. TsNIGRI,* 1979, vol. 149, pp. 53–56.

Savva, N.E., *Mineralogiya serebra Severo-Vostoka Rossii* (Silver Mineralogy of Northeast Russia), Moscow: "Triumf", 2019.

Shilo, N.A., Sakharova, M.S., Krivitskaya, N.N., Ryakhovskaya, S.K., and Bryzgalov, I.A., *Mineralogiya i geneticheskie osobennosti zoloto–serebryanogo orudeneniya Severo-Zapadnoi chasti Tikhookeanskogo obramleniya* (Mineralogy and Genetic Features of the Gold–Silver Mineralization of the Northwestern Pacific Margin), Moscow: Nauka, 1992.

Shpikerman, V.I., *Domelovaya minerageniya Cevero–Vostoka Azii* (Pre–Cretaceous Metallogeny of Northeast Asia), Magadan: SVKNII DVO RAN, 1998.

Stepanov, V.A. and Shishakova, L.N., *Kubakinskoe zolotoserebryanoe mestorozhdenie* (Kubaka Gold–Silver Deposit), Vladivostok: Dal'nauka, 1994.

Taylor, S.R. and McLennan, S.M., *The Continental Crust: its Composition and Evolution* (Blackwell Scientific Publications, 1985).

Vinokurov, S.F., Kovalenker, V.A., Safonov, Yu.G., and Kerzin, A.L., REE in quartz from epithermal gold deposits: distribution and genetic implications, *Geochem. Int.,* 1999, vol. 37, no. 2, pp. 145–152.

Volkov, A.V., Savva, N.E., Kolova, E.E., Prokof'ev, V.Yu., and Murashov, K.Yu., Dvoinoe Au–Ag epithermal deposit, Chukchi Peninsula, Russia, *Geol. Ore Deposits,* 2018, vol. 60, no. 6, pp. 527–546.

Volkov, A.V., Savva, N.E., and Sidorov, A.A., Au and Ag metallogeny of the Kedon volcanic–plutonic belt (D_{2-3}) (Northeast Russia), *Dokl. Earth Sci.,* 2011, vol. 439, no. 2, pp. 1063–1069.

Volkov, A.V., Sidorov, A.A., Savva, N.E., Kolova, E.E., Murashov, K.Yu., and Zemskova, M.I., Epithermal mineralization in the Kedon Paleozoic volcano-plutonic belt, Northeast Russia: geochemical studies of Au–Ag mineralization, *J. Volcanol. Seismol.,* 2017, vol. 11, no. 1, pp. 1–19.

Yushko-Zakharova, O.E., Ivanov, V.V., Soboleva, L.N., Dubakina, L.S., Shcherbachev, D.K., Kulichikhina, R.D., and Timofeeva, O.S., *Mineraly blagorodnykh metallov: Spravochnik* (Noble Metal Minerals. A Textbook), Moscow: Nedra, 1986.

Zharikov V.A., Gorbachev N.S., Lightfoot, P., and Doherty, W., Rare earth element and yttrium distribution between fluid and basaltic melt at pressures of 1–12 kbar: evidence from experimental data, *Dokl. Earth Sci.,* 1999. T. 366, no. 4, pp. 543–545.

Translated by E. Murashova